Title

Principal Component Analysis of Simultaneous PET-MRI Reveals Patterns of Bone—Cartilage Interactions in Osteoarthritis

Journal

Journal of Magnetic Resonance Imaging, 52(5)

ISSN

1053-1807

Authors

Tibrewala, Radhika
Pedoia, Valentina
Bucknor, Matthew
et al.

Publication Date

2020-11-01

DOI

10.1002/jmri.27146

Peer reviewed

HHS Public Access

Author manuscript

J Magn Reson Imaging. Author manuscript; available in PMC 2024 May 13.

Published in final edited form as:

J Magn Reson Imaging. 2020 November ; 52(5): 1462–1474. doi:10.1002/jmri.27146.

Principal Component Analysis of Simultaneous PET-MRI Reveals Patterns of Bone–Cartilage Interactions in Osteoarthritis

Radhika Tibrewala, MS[*], **Valentina Pedoia, PhD**,
Matthew Bucknor, MD,
Sharmila Majumdar, PhD

Department of Radiology and Biomedical Imaging, University of California, San Francisco, California, USA

Abstract

Background: Bone–cartilage interactions have been implicated in causing osteoarthritis (OA).

Purpose: To use [^{18}F]-NaF PET-MRI to 1) develop automatic image processing code in MatLab to create a model of bone–cartilage interactions and 2) find associations of bone–cartilage interactions with known manifestations of OA.

Study Type: Prospective study aimed to evaluate a data analysis method.

Population: Twenty-nine patients with knee pain or joint stiffness.

Field Strength/Sequence: 3T MRI (GE), 3D CUBE FSE, 3D combined $T_{1\rho}/T_2$ MAPSS, [18F]-sodium fluoride, SIGNA TOF (OSEM).

Assessment: Correlation between MRI (cartilage) and PET (bone) quantitative parameters, bone–cartilage interactions model described by modes of variation as derived by principal component analysis (PCA), WORMS scoring on cartilage lesions, bone marrow abnormalities, subchondral cysts.

Statistical Tests: Linear regression, Pearson correlation.

Results: Mode 1 was a positive predictor of the bone abnormality score ($P = 0.0003$, $P = 0.001$, $P = 0.0007$) and the cartilage lesion score ($P = 0.03$, $P = 0.01$, $P = 0.02$) in the femur, tibia, and patella, respectively. For the cartilage lesion scores, mode 5 was the most important positive predictor in the femur ($P = 3.9E-06$), and mode 2 were predictors, significant negative predictor in the tibia ($P = 0.007$). In the patella, mode 1 was a significant positive predictor of the bone abnormality score ($P = 0.0007$).

Data Conclusion: By successfully building an automatic code to create a bone–cartilage interface, we were able to observe dynamic relationships between biochemical changes in the cartilage accompanied with bone remodeling, extended to the whole knee joint instead of simple colocalized observations, shedding light on the interactions that occur between bone and cartilage in OA.

[*]Address reprint correspondence to: R.T., 1700 4th St, Suite 203, San Francisco, 94158, CA, USA. radhika.tibrewala@ucsf.edu.

Evidence Level: 3

Technical Efficacy: Stage 3

Osteoarthritis (OA) is a chronic, debilitating joint disorder that is expected to affect more people due to the aging of the population and the obesity epidemic. OA causes joint stiffness, pain and loss of mobility, and is characterized by cartilage destruction, subchondral bone changes, osteophyte formation, and other complex pathological changes that are not clearly understood despite its widespread prevalence and high costs to the economy.[2,3] Although cartilage destruction is a characteristic feature of OA, it has been recognized that OA is a whole-joint disease. The interactions between cartilage and subchondral bone have been thought to be important in causing OA.[5] The interface between cartilage and bone is a unique loading zone, and well-defined progressive destructive changes in the cartilage have been found to parallel changes in the underlying bone.[5] It has been suggested that increased vascularization in joints during OA facilitate movements of molecules from bone to cartilage and vice versa.[6]

Imaging plays an important role in diagnosing OA. Currently, OA diagnosis is defined by joint space narrowing (JSN) and osteophytes that are visible on radiographs, graded according to Kellgren–Lawrence scores.[7] However, early changes in cartilage and bone like collagen network disruption due to proteoglycan depletion, bone remodeling in the subchondral and trabecular bone, which are implicated in the bone–cartilage crosstalk, are not seen on radiographs.[8] Thus, magnetic resonance imaging (MRI) has been used to investigate cartilage degeneration biomarkers using MRI-based $T_{1\rho}$ and T_2 relaxation times, which assess proteoglycan and collagen content in cartilage, respectively, and these have been found to have differences between normal and OA patients.[9–11] Additionally, [^{18}F]-NaF (sodium fluoride) positron emission tomography (PET)-MRI has previously been used in investigating bone–cartilage relationships, owing to its simultaneous functional and structural imaging capabilities, proving itself a feasible method to study early OA.[12–15] 18-Fluoride (18-F) is a highly sensitive bone imaging agent that is extracted by the blood system in the body in proportion to the osteoblastic activity (reflecting blood flow and bone remodeling), and has been used as a PET tracer for multiple musculoskeletal diseases, including OA.[16–18] Savic et al found that increases in cartilage $T_{1\rho}$ relaxation times (indicating degenerative changes) were associated with increased turnover in the adjoining bone as imaged by [^{18}F]-NaF.[14] Kogan et al found higher standardized uptake values (SUVs) in bone where there were bone marrow edemas, osteophytes, and sclerosis compared to normal-appearing bone.[12] Kobayashi et al and Draper et al found that not all increased uptakes corresponded to structural abnormalities on MRI, suggesting that NaF-PET can detect bone abnormalities even before MRI.[15,19] Tibrewala et al found direct associations between quantitative MRI and PET evidence of bone remodeling in hip OA.[13] In a study of anterior cruciate ligament (ACL)-injured patients using PETMRI, Kogan et al found increased tracer uptake and cartilage T_2 relaxation in ACL-reconstructed knees, as compared to the contralateral knees. Moreover, they observed a spatial relationship between cartilage T_2 and SUV, where increased tracer uptake in the subchondral bone adjacent to an area of increased cartilage relaxation time was observed.[20]

While all these studies have found important and direct evidence of associations between cartilage degeneration and neighboring bone changes, these have mostly been performed by calculating mean, maximum values of SUV in regions of bone abnormalities and those surrounding cartilage lesions. Evidence of colocalized relationships between bone remodeling and cartilage degeneration has been offered. Since the knee is a complex joint, only studying associations between bone changes and surrounding cartilage degeneration biomarkers would miss potential, multifaceted mechanisms that are not spatially correlated in the joint, but are part of the more complex bone–cartilage interaction that has been suggested as a mechanism in OA.[5]

In order to use [^{18}F]-NaF PET-MRI to investigate the bone–cartilage crosstalk that is implicated in causing OA, the goals of this study were: 1) develop automatic image processing code that helps to create a model of bone–cartilage interactions using simultaneously acquired [^{18}F]-NaF PET-MRI data, and 2) find associations of bone–cartilage interactions with known manifestations of OA.

Materials and Methods

The study was approved by the local Institutional Review Board (IRB) and written informed consent was obtained from all subjects before the study.

Patient Population

All the personnel involved with recruitment, scanning, and analysis of this study were HIPAA (Health Insurance Portability and Accountability Act)-compliant. Radiographs were obtained prior to the study and Kellgren–Lawrence (KL)[7] grading of the radiographs was performed by a board-certified musculoskeletal radiologist (M.B.) with more than 10 years of experience to stage the extent of knee OA. The inclusion criteria were age >35 years, knee pain or ache, or stiffness in the joint most days of the month. The exclusion criteria were any concurrent use of an investigational drug, history of fracture in the knee, history of surgery in the knee, or contraindications to MRI.

PET-MR Image Acquisition

Image acquisition was performed with a SIGNA 3T time of flight (TOF) PET-MRI (GE Healthcare, Milwaukee, WI). The timing resolution of this scanner as per the manufacturer was less than 400 ps. PET images were reconstructed by a TOF OSEM algorithm (four iterations; 28 subsets; axial field of view [FOV] 500 mm; matrix size 256 × 256 × 89; voxel size 1.95 × 1.95 × 2.78 mm^3).

Subjects were positioned supine feet-first, with a medium-size receiver flex coil wrapped around the knee of interest in the PET-MRI scanner. [^{18}F]-NaF was used as a tracer, sourced from our institutional cyclotron facility, produced using current good manufacturing practices (cGMP) guidelines. An average dose of 294.87 ⍺ 59.78 (range 191.20–370) MBq of [^{18}F]-NaF was imparted to each patient for a dynamic PET scan of 60 minutes, with MRI sequences running concurrently. An effective dose of 0.024 mSv/MBq was used to calculate the radiation exposure to each subject due to the injected [^{18}F]-NaF.[18] A Dixon fat–water sequence was acquired for MR-based attenuation correction (MRAC) of PET photons.[21] The

MR images acquired simultaneously with PET included: 1) 3D isotropic CUBE FSE, and 2) 3D sagittal combined $T_{1\rho}/T_2$. MRI acquisition parameters are shown in Table 1.

MRI Morphologic Grading

Semiquantitative WORMS[22] grading was used by a board-certified radiologist (M.B.) with 10+ years of experience for assessing morphological abnormalities in the recruited patients on the 3D isotropic CUBE images (Table 1), acquired in the sagittal plane. Briefly described, cartilage lesions were graded on an 8-point scale that incorporates the cartilage thickness loss, focal defect, and signal abnormality on different levels. Bone marrow abnormalities were graded on a 4-point scale based on the amount of areas of increased signal and subarticular cysts were graded on a 4-point scale based on the extent of regional involvement.

Image Processing and Building the Bone–Cartilage Interactions Model

Image analysis (Fig. 1) was performed automatically using an inhouse program developed in MatLab (MathWorks, Natick, MA). For the combined $T_{1\rho}/T_2$sequences, a previously validated[23] nonrigid registration of all images was performed on a reference space that was selected as a patient with average body mass index (BMI) and age. $T_{1\rho}$and T_2maps were obtained by fitting the images obtained with different time of spin lock (TSL) and echo time (TE) using a Levenberg–Marquardt monoexponential $\left(S(TSL) \propto e^{-TSL/T1\rho}\right)$, applied to each voxel. The cartilage segmentation, which was performed manually on the reference space, was then applied to the $T_{1\rho}$ and T_2 maps to obtain $T_{1\rho}$ and T_2 values in the six cartilage compartments (medial femoral condyle [MFC], medial tibia [MT], lateral femoral condyle [LFC], lateral tibia [LT], femoral trochlea [TRO], and patella [PAT]) for each patient.[23]

For the PET-MR images, MR images were acquired in the sagittal plane, while PET images were acquired in the axial plane for greater coverage. The axial PET data were first resampled into the $T_{1\rho}$ (sagittal) coordinates to transform all the PET images into the same orientation and coverage as the MR images. PET data were converted into SUV maps by using the patients' weight and injected tracer activity.[24]

Point-by-Point Pearson Correlations

MRI metrics ($T_{1\rho}$,T_2) were measured on the cartilage, while PET metrics (SUV) were measured on the bone. Thus, $T_{1\rho}$, T_2, and SUV were projected onto a common interface at the bone–cartilage surface intersection using the following method: for each point along the interface, a trajectory perpendicular to it was first determined, and the value of the respective parameter ($T_{1\rho}$, T_2, and SUV) along this trajectory across the adjacent cartilage was then averaged and assigned to the corresponding point on the interface. For the SUV within the bone, regions of interest (ROIs) encompassing the subchondral bone (9-mm-thick, starting from the cartilage) were manually defined on the reference for each knee compartment.[25] The SUVs along the trajectory inside the bone and limited to this region were averaged and assigned to the corresponding point on the interface, resulting in a bone–cartilage interface containing values of $T_{1\rho}$, T_2, and SUV. Additionally, $T_{1\rho}$, T_2 values for each patient were averaged in each cartilage compartment, and SUVs within each bone (femur, tibia, patella)

in an ROI in the bone near the respective cartilage (defined on the reference space) were averaged for each patient, to find the mean and standard deviation of $T_{1\rho}$, T_2, and SUV values in each patients' knee compartments.

After building the interface, with all the SUV, $T_{1\rho}$, T_2 values projected on the same space, a point-by-point Pearson correlation map (between $T_{1\rho}$, T_2, and SUV, $T_{1\rho}$, and SUV,T_2) was built for the femur, tibia, and patella bones. The percentage of voxels with significant positive and negative correlations ($P < 0.05$) (between $T_{1\rho}$, T_2, and SUV, $T_{1\rho}$, and SUV,T_2), within each cartilage compartment were calculated and reported.

Modeling Simultaneous Bone–Cartilage Interactions

For each patient, the $T_{1\rho}$ and SUVs from the interface were flattened to a 2D vector and then combined (Eqs. 1–3), where each value of $T_{1\rho}$ and SUV corresponded to a specific voxel as defined on the reference space:

$$Bone_{interface} = \begin{bmatrix} x_1 & y_1 & z_1 & SUV_1 \\ x_2 & y_2 & z_2 & SUV_2 \\ .. & .. & .. & .. \\ x_n & y_n & z_n & SUV_n \end{bmatrix} \quad (1)$$

$$Cartilage_{interface} = \begin{bmatrix} x_1 & y_1 & z_1 & T1\rho_1 \\ x_2 & y_2 & z_2 & T1\rho_2 \\ .. & .. & .. & .. \\ x_n & y_n & z_n & T1\rho_n \end{bmatrix} \quad (2)$$

$$BoneCartilage_{interface} = \begin{bmatrix} x_1 & y_1 & z_1 & SUV_1 & T1\rho_1 \\ x_2 & y_2 & z_2 & SUV_2 & T1\rho 2 \\ .. & .. & .. & .. & .. \\ x_n & y_n & z_n & SUV_n & T1\rho_n \end{bmatrix} \quad (3)$$

where $n$is the number of points in the bone–cartilage interface (which is the same for each patient due to the common reference registration applied on all patients). These input feature vectors (Eq. 3) of all the patients were concatenated to create a matrix (Eq. 4) that consisted of the location of each voxel followed by its $T_{1\rho}$ and SUV for all the patients:

$$BoneCartilage^{all}_{interface} = \begin{bmatrix} x_1 & y_1 & z_1 & SUV_1^1 & T1\rho_1^1 & SUV_1^2 & T1\rho_1^2 & .. & SUV_1^k & T1\rho_1^k \\ x_2 & y_2 & z_2 & SUV_2^1 & T1\rho_2^1 & SUV_2^2 & T1\rho_2^2 & .. & SUV_2^k & T1\rho_2^k \\ .. & .. & .. & .. & .. & .. & .. & .. & .. & .. \\ x_n & y_n & z_n & SUV_n^1 & T1\rho_n^1 & SUV_n^2 & T1\rho_n^2 & .. & SUV_n^k & T1\rho_n^k \end{bmatrix} \quad (4)$$

where $n$is the number of points in the bone–cartilage interface and k is the number of patients. The voxel locations were removed since they were the same for all patients (the patients were all registered on the reference space). This process was performed for all the cartilage compartments, and the matrices of the cartilage compartments belonging to one bone were combined (eg, MFC, LFC, and TRO). Therefore, a total of three matrices were constructed, one for each bone. The $T_{1\rho}$ and SUV data were normalized (in a 0–1 range) by the sum of its mean and three times the standard deviation, computed across all the patients, after removing any zeros that were present in the data.

Principal component analysis (PCA) was used to find patterns of interactions between $T_{1\rho}$ and SUV,[26] using these matrices as inputs. PCA is a technique that is used to reduce the dimensionality of datasets and extract relevant patterns in the data while retaining interpretability and minimizing information loss. Unsupervised dimensionality reduction techniques such as PCA and ICA have been used in applications of diagnostic PET patterns in Parkinson's and normal aging[27,28] and have been widely used to study brain network connections,[29] but the applications on multimodal musculoskeletal imaging are still very limited. Habeck et al, when using PCA to study PET data for Alzheimer's disease, state that PCA is able to identify covariance patterns that signal the disease onset even when there is no spatial correlation between distant regions.[30] PCA is thus able to identify unexpected patterns that lie in the data, which are not seen with traditional PET data analysis methods.

Thus, to perform PCA, eigenvalue and eigenvector decomposition of the correlation matrices of the inputs (Eq. 4 with normalization and voxel location removal) were used to extract principal components (PCs) to calculate the most important modes of variations of the $T_{1\rho}$ and SUVs. Each PC described a different pattern of change in both $T_{1\rho}$ and SUV, and therefore the $T_{1\rho}$ and SUVs of each patient were described by a linear combination of these patterns. For each patient the coefficients of the linear combination of the first five PCs were considered in the analysis. For each patient those PC scores represent the similarity between the $T_{1\rho}$ and SUV PC pattern and the specific patient $T_{1\rho}$ and SUV pattern. The interpretation of each PC was investigated by changing its value of the PC scores from mean to mean 5 α SDs and observing the changes in pattern of $T_{1\rho}$ and SUV mapped on the reference space for each bone.

Statistical Analysis

To check if the patterns of interaction in the bone–cartilage interface derived using PCA could predict known manifestations of OA, a stepwise linear regression model was built to predict the cartilage lesion score and bone (sum of bone marrow abnormalities and cyst scores) scores from the scores of the first five modes of variation of each patient. For comparison with standard analysis and to understand the value of the proposed method, the same linear model was built using average $T_{1\rho}$ and average SUV values of all the compartments in the knee as possible predictors. In all regression models, age, gender, and BMI of the patients were adjusted ($P < 0.05$). All statistical analysis was carried out in MatLab (MathWorks).

Results

Patient Population and MRI Morphological Characteristics

Twenty-nine patients were recruited for this study with age 55.90 ± 8.60 years, BMI 25.14 ± 3.45 Kg/m^3, 33.33% females, 64% KL 0–1, 14% KL = 2, and 22% KL = 3.[7] As seen in Fig. 2, the WORMS scores showed that most patients had cartilage lesions in the patella (57% of patients) and trochlea (43% of patients), with correspondingly high mean $T_{1\rho}$ values (45.28 ± 8.64 msec in patella and 43.32 ± 6.44 msec in trochlea) and mean T_2 values (32.76 ± 8.33 msec in patella and 32.49 ± 4.68 msec in trochlea). Similarly, most patients had cysts in the patella (21% of patients) and trochlea (21% of patients), and edematous bone marrow lesions in the patella (21% of patients) and trochlea (10% of patients), with correspondingly high mean SUVs (0.76 ± 0.80 in patella and 0.62 ± 0.78 in trochlea). As seen, the mean SUVs in all the compartments have high SDs, showing a large spread of tracer uptake in each compartment throughout the dataset.

Point-by-Point Pearson Correlations

Figure 3 shows maps of point-by-point correlations between $T_{1\rho}$ and T_2, $T_{1\rho}$, and SUV and T_2 and SUV. The values are all derived after projecting the $T_{1\rho}$, T_2, and SUVs onto the bone–cartilage interface as described in Materials and Methods. Strong positive correlations are seen between $T_{1\rho}$ and T_2 values in all three bones, femur, tibia, and patella spread in all the cartilage compartments. Table 2 shows the percentage of voxels within each cartilage compartment that had significant ($P < 0.05$) positive or negative correlations between $T_{1\rho}$ and T_2, $T_{1\rho}$, and SUV and T_2 and SUV. As seen in Table 2 and Fig. 3, over 95% of voxels in all cartilage compartments displayed significant positive correlations between $T_{1\rho}$ and T_2. In the femur, the lateral cartilage compartment contained 13% of voxels that had significant positive associations between $T_{1\rho}$ and SUV as compared to the medial cartilage compartment that had 4% of voxels that had significant positive associations between $T_{1\rho}$ and SUV. Similarly, in the tibia, the lateral cartilage compartment contained 45% of voxels that had significant positive associations between $T_{1\rho}$ and SUV as compared to the medial cartilage compartment that had 5% of voxels that had significant positive associations between $T_{1\rho}$ and SUV. In the femur, the lateral cartilage compartment contained 16% of voxels that had significant positive associations between T_2 and SUV as compared to the medial cartilage compartment that had 8% of voxels that had significant positive associations between T_2 and SUV. Similarly, in the tibia, the lateral cartilage compartment contained 53% of voxels that had significant positive associations between T_2 and SUV as compared to the medial cartilage compartment that had 6% of voxels that had significant positive associations between T_2 and SUV. Very few voxels with negative correlations were seen between any given pair of values.

Modes of Variation Derived Using PCA

Since the $T_{1\rho}$ and T_2 maps were found to be highly correlated, T_2values were not included in the PCA when extracting the modes of variation. Between $T_{1\rho}$ and T_2, $T_{1\rho}$was chosen to be retained in the PCA because it has been proposed as a more specific indicator of

proteoglycan content in cartilage as compared to T_2, and therefore was more sensitive to changes in proteoglycan in the cartilage matrix during early OA development. Furthermore, there is a larger range of $T_{1\rho}$ values, making it more sensitive to cartilage degeneration.[10]

The first five modes derived using PCA described 84%, 86%, and 91% of the overall variation in femur, tibia, and patella, respectively. These modes that depict the different bone–cartilage interactions by using the $T_{1\rho}$ and SUVs projected onto the same space were extracted using PCA and explored for each bone separately (femur, tibia, patella).

Associations of Patterns of Interactions Between $T_{1\rho}$ and SUVs Derived by PCA With Cartilage and Bone Abnormality Scores

As seen in Table 3, all of the models were significant ($P < 0.001$) in using the modes of interaction between $T_{1\rho}$ and SUVs derived by PCA to predict cartilage and bone abnormalities. Table 3 shows that mode 1 was a positive predictor of the bone abnormality score ($P = 0.0003$, $P = 0.001$, $P = 0.0007$) and the cartilage lesion score ($P = 0.03$, $P = 0.01$, $P = 0.02$) in the femur, tibia, and patella, respectively. For the cartilage lesion scores, mode 5 was the most important positive predictor in the femur ($P = 3.9E\text{-}06$), and mode 2 were predictors, significant negative predictor in the tibia ($P = 0.0007$). In the patella, only mode 1 was retained in the regression model, and was a significant positive predictor of the bone abnormality score ($P = 0.0007$).

These modes that showed associations with total cartilage lesion and bone abnormality scores are visualized in Fig. 4. In the femur, mode 1 showed increased SUV in the trochlea with a small change in $T_{1\rho}$ in the same region. Additionally, mode 1 showed a higher SUV uptake in the outer (more lateral) side of each cartilage compartment as compared to the inner (more medial) side. This mode showed a positive association with the cartilage lesion score ($P = 0.03$) and the bone abnormality score ($P = 0.0003$). Mode 4 depicted an elevation of SUV in a different region of trochlea (compared to mode 1), with a corresponding reduction in the medial femoral cartilage $T_{1\rho}$ values. When interacting with mode 1, this mode was a positive significant ($P = 0.03$) predictor of bone abnormality scores. In mode 5, an increase in lateral femoral cartilage $T_{1\rho}$ and an SUV increase right adjacent to it was observed. This mode was the most significant positive predictor of the cartilage lesion score ($P = 3.9E\text{-}06$) and the bone abnormality score ($P = 0.0002$). In the tibia, mode 1 showed an increase of $T_{1\rho}$ in the lateral tibial cartilage, and a simultaneous increase in SUV distributed through the lateral cartilage. Similar to the first mode of the femur, mode 1 of the tibia also showed a higher SUV uptake in the outer (more lateral) side of each cartilage compartment as compared to the inner (more medial) side. This mode was a positive significant predictor of cartilage lesion scores ($P = 0.01$) and bone abnormality score ($P = 0.001$). Mode 2 showed a reduction in SUV in the medial tibial cartilage and an increase of SUV in the lateral tibia cartilage accompanied by an increase of $T_{1\rho}$ in the lateral cartilage. This mode was a significant negative predictor of cartilage lesion scores ($P = 0.007$) and bone abnormality score ($P = 0.001$). In the patella, only $T_{1\rho}/T_2$ MAPSS sequence for patients that had minimum and maximum values of the modes derived by the PCA that were found to be predictors of manifestations of OA. In the femur, the patient with the smallest value of mode 1 had a normal range of $T_{1\rho}$ values in the trochlea as compared to the patient with the biggest value

of mode 1. The patient with the largest value of mode 1 also depicted a lot of tracer uptake in the femur as compared to the other patient, and this uptake was found to be adjacent to the cartilage with the elevated $T_{1\rho}$ values. In mode 4 of the femur, between the minimum and maximum value patient, there is a small reduction in $T_{1\rho}$ in the medial femoral cartilage, but it is spatially distributed, along with a small increase in SUV in the femur near the weight-bearing region. In mode 5, there is a visible increase in $T_{1\rho}$ in the lateral femoral cartilage. In the tibia, between the minimum value and maximum value patient of mode 1, there is an elevation in the lateral tibia cartilage $T_{1\rho}$ accompanied with an increase in SUV in the same region of the tibia. In mode 2, there is a reduction of SUV in the medial tibia, and not much change in the medial tibia cartilage. Finally, in mode 1 of the patella, the maximum value patient shows a very sharp increase of both $T_{1\rho}$ and SUV in the patella cartilage and bone, respectively, as compared to the minimum value patient.

Discussion

This study demonstrated the ability of [^{18}F]-NaF PET-MRI and principal component analysis to image bone–cartilage PAT = patella. interactions in the knee for OA. Using PCA, direct associations between quantitative PET-MRI parameters and WORMS scoring were found in the femur, tibia, and patella.

Our study showed that using the mean values of the $T_{1\rho}$ and SUV of all the patients in ROIs in a regression model were able to predict the bone and cartilage lesion scores. However, using the PCA went one step further in actually combining the $T_{1\rho}$ and SUV concurrently in the same region and also across the joint, therefore interpreting a more comprehensive bone–cartilage interaction, and not isolating PET or MRI quantitative parameters to colocalized correlations. Thus, PCA was able to identify patterns in the data that were not seen with the averaging methods. Furthermore, the results showed that the regression models were stronger in the PCA as compared to the mean values based on their R-square values, which showed that a combination of the $T_{1\rho}$ and SUV (the modes of variation) were able to account for more of the variance in the data as compared to each individually.

In this study, mode 1 was found to be akin to the results of the point-by-point correlations, which was expected, since this is the largest variation in the data in all three bones. Interestingly, in the femur and tibia, mode 1 depicted a pattern that showed that SUV was higher in the outer regions (more lateral) of the cartilage as compared to the inner regions (more medial) of the cartilage. Since this pattern was observed in the first mode of both the bones, it was present in a higher proportion of the dataset. Additionally, since it was also positively predictive of the cartilage and bone abnormalities, it could show that a difference in loading of the outer vs. inner portions of the cartilage have an effect on the morphological changes observed in the patients. Since these are early OA patients, it could also show that bone remodeling near the outer cartilage regions precedes that in the inner cartilage regions. Previous studies have explored the differences between the superficial and deep layers of the cartilage, modeling how the cartilage biochemical composition changes as it moves away from the surface of the bone (top to bottom within the cartilage).[20,31,32] However, the change in cartilage composition from a medial to lateral direction within one cartilage, (left

to right within cartilage) has not been explored as well. The results of mode 1 show that this method is feasible in exploring these differences. Mode 5 of the femur was found to be the most important predictor of the cartilage and bone abnormalities. This mode depicted a sharp increase in $T_{1\rho}$ and SUV in the lateral cartilage of the femur. This result provides new insights into the pathophysiology of OA, since OA is known to most commonly affect the medial compartment of the knee.[33] One reason for this could be that this study's dataset was biased, since there were more lesions on the lateral side. Another possible explanation for this could be that the mechanisms of medial and lateral compartment loading in OA differ in a way that involves less interaction between the bone and cartilage (less in the medial side), and was therefore not observed in this study. The conformity of the tibiofemoral joint surface has been shown previously to differ with sex,[34] and furthermore, impact the wear performance after total knee replacement.[35] This conformity could also impact the shear loading at the medial knee compartment, and have an effect on the mechanism of OA. Mode 2 of the tibia showed that an SUV increase in the lateral region was concurrent with an SUV reduction in the medial region. This mode showed the behavior of bone remodeling in different regions of the knee. OA is hypothesized to be initiated by alterations in normal knee kinematics that shift loading from regions of cartilage that are more suited for loading rather than those that are not.[33] A previous study has also found varying uptake of [^{18}F]-NaF in response to bone loading,[36] but these were observed as effects of immediate loading and not a gradual change a bone due to abnormal joint loading. Specifically, the result of mode 2 in tibia shows the feasibility of this [^{18}F]-NaF PET-MRI method using PCA to model and image bone–cartilage interactions that could be caused as a result of altered loading.

Limitations

First, these observations were made in a cohort of 29 patients, and a larger patient population would be needed to make more generalizable observations. Second, while PCA was useful in finding these new patterns of interaction between bone and cartilage, the interpretation of the modes is completely visual, and certain interactions may have been missed. PCA is also sensitive to outliers, and thus will perform better on a larger, well-distributed heterogeneous dataset. In a study of ACL injured knees, Kogan et al observed differences in subchondral bone SUV in deep and superficial layers of the cartilage.[20] In this initial method study, we projected $T_{1\rho}$ relaxation times along the entire thickness of the cartilage on the bone–cartilage interface. For future directions, a split of the cartilage into deep and superficial layers would be useful in determining differences of SUV corresponding to MRI-based relaxation times in different layers of the cartilage. While in this study we chose a thickness of 9 mm on the template patients' bone ROI, in future studies we would also perform more studies to find the difference when projecting the tracer uptake from ROIs of different thickness in the bone, to see if that changes the patterns of interactions observed between bone and cartilage. Plus, for future studies, we will incorporate the dynamic PET data to establish differences in blood flow to the bone during these observed bone remodeling changes. A longitudinal study would help in determining the evolution of these observed bone–cartilage interactions, and furthermore determine the origination of pain that is manifested in OA.

Conclusion

Nevertheless, in this study we built a bone–cartilage interface and observed concurrent interactions between the two in the knee joint of patients with OA using PCA. By building a bone–cartilage interface, we were able to observe dynamic relationships between biochemical changes in the cartilage accompanied with bone remodeling, extended to the whole knee joint instead of simple colocalized observations. We were able to probe pathological changes with PET imaging, and observe structural changes using MRI, unleashing the potential for targeted treatment and early diagnosis using areas of bone remodeling and cartilage degeneration.[37]

Supplementary Material

Refer to Web version on PubMed Central for supplementary material.

Acknowledgments

We thank Emma Bahroos, Hatef Mehrabian, and Dragana Savic for their help with image acquisition.

The authors acknowledge the funding sources and research grants from GE Healthcare.

References

1. Zhang Y, Jordan JM. Epidemiology of osteoarthritis. Clin Geriatr Med 2010;26(3):355–369. [PubMed: 20699159]
2. Herrero-Beaumont G, Roman-Blas JA, Bruyere O, et al. Clinical settings in knee osteoarthritis: Pathophysiology guides treatment. Maturitas 2017;96:54–57. [PubMed: 28041596]
3. Deshpande BR, Katz JN, Solomon DH, et al. Number of persons with symptomatic knee osteoarthritis in the US: Impact of race and ethnicity, age, sex, and obesity. Arthritis Care Res (Hoboken) 2016;68(12):1743–1750. [PubMed: 27014966]
4. Lespasio MJ, Piuzzi NS, Husni ME, Muschler GF, Guarino A, Mont MA. Knee osteoarthritis: A primer. Perm J 2017;21:16–183.
5. Findlay DM, Kuliwaba JS. Bone-cartilage crosstalk: A conversation for understanding osteoarthritis. Bone Res 2016;4:16028. [PubMed: 27672480]
6. Sharma AR, Jagga S, Lee SS, Nam JS. Interplay between cartilage and subchondral bone contributing to pathogenesis of osteoarthritis. Int J Mol Sci 2013;14(10):19805–19830. [PubMed: 24084727]
7. Kellgren JH, Lawrence JS. Radiological assessment of osteo-arthrosis. Ann Rheum Dis 1957;16(4):494–502. [PubMed: 13498604]
8. Burr DB, Gallant MA. Bone remodelling in osteoarthritis. Nat Rev Rheumatol 2012;8(11):665–673. [PubMed: 22868925]
9. David-Vaudey E, Ghosh S, Ries M, Majumdar S. T2 relaxation time measurements in osteoarthritis. Magn Reson Imaging 2004;22(5): 673–682. [PubMed: 15172061]
10. Li X, Benjamin Ma C, Link TM, et al. In vivo T(1rho) and T(2) mapping of articular cartilage in osteoarthritis of the knee using 3 T MRI. Osteoarthr Cartil 2007;15(7):789–797.
11. Li X, Han ET, Busse RF, Majumdar S. In vivo T(1rho) mapping in cartilage using 3D magnetization-prepared angle-modulated partitioned kspace spoiled gradient echo snapshots (3D MAPSS). Magn Reson Med 2008;59(2):298–307. [PubMed: 18228578]
12. Kogan F, Fan AP, McWalter EJ, Oei EHG, Quon A, Gold GE. PET/MRI of metabolic activity in osteoarthritis: A feasibility study. J Magn Reson Imaging 2017;45(6):1736–1745. [PubMed: 27796082]

13. Tibrewala R, Bahroos E, Mehrabian H, et al. [(18) F]-sodium fluoride PET/MR imaging for bone-cartilage interactions in hip osteoarthritis: A feasibility study. J Orthop Res 2019;37(12):2671–2680. [PubMed: 31424110]
14. Savic D, Pedoia V, Seo Y, et al. Imaging bone-cartilage interactions in osteoarthritis using [(18)F]-NaF PET-MRI. Mol Imaging 2016;15:1–12. [PubMed: 28654417]
15. Kobayashi N, Inaba Y, Tateishi U, et al. Comparison of 18F-fluoride positron emission tomography and magnetic resonance imaging in evaluating early-stage osteoarthritis of the hip. Nucl Med Commun 2015;36(1):84–89. [PubMed: 25230054]
16. Segall G, Delbeke D, Stabin MG, et al. SNM practice guideline for sodium 18F-fluoride PET/CT bone scans 1.0. J Nucl Med 2010;51(11): 1813–1820. [PubMed: 21051652]
17. Al-Zaghal A, Raynor W, Khosravi M, Guermazi A, Werner TJ, Alavi A. Applications of PET imaging in the evaluation of musculoskeletal diseases among the geriatric population. Semin Nucl Med 2018;48(6): 525–534. [PubMed: 30322478]
18. Jadvar H, Desai B, Conti PS. Sodium 18F-fluoride PET/CT of bone, joint, and other disorders. Semin Nucl Med 2015;45(1):58–65. [PubMed: 25475379]
19. Draper CE, Quon A, Fredericson M, et al. Comparison of MRI and (1)(8) F-NaF PET/CT in patients with patellofemoral pain. J Magn Reson Imaging 2012;36(4):928–932. [PubMed: 22549985]
20. Kogan F, Fan AP, Monu U, Iagaru A, Hargreaves BA, Gold GE. imaging of bone-cartilage interactions in ACL-injured patients with PET-MRI. Osteoarthr Cartil 2018;26(6):790–796.
21. Wagenknecht G, Kaiser HJ, Mottaghy FM, Herzog H. MRI for attenuation correction in PET: Methods and challenges. MAGMA 2013;26(1): 99–113. [PubMed: 23179594]
22. Peterfy CG, Guermazi A, Zaim S, et al. Whole-organ magnetic resonance imaging score (WORMS) of the knee in osteoarthritis. Osteoarthr Cartil 2004;12(3):177–190.
23. Pedoia V, Gallo MC, Souza RB, Majumdar S. Longitudinal study using voxel-based relaxometry: Association between cartilage T1rho and T2 and patient reported outcome changes in hip osteoarthritis. J Magn Reson Imaging 2017;45(5):1523–1533. [PubMed: 27626787]
24. Kinahan PE, Doot RK, Wanner-Roybal M, et al. PET/CT assessment of response to therapy: Tumor change measurement, truth data, and error. Transl Oncol 2009;2(4):223–230. [PubMed: 19956382]
25. Hirvasniemi J, Thevenot J, Guermazi A, et al. Differences in tibial subchondral bone structure evaluated using plain radiographs between knees with and without cartilage damage or bone marrow lesions — The Oulu Knee Osteoarthritis study. Eur Radiol 2017;27(11):4874–4882. [PubMed: 28439649]
26. Jolliffe IT, Cadima J. Principal component analysis: A review and recent developments. Philos Trans A Math Phys Eng Sci 2016;374(2065): 20150202.
27. Brickman AM, Habeck C, Zarahn E, Flynn J, Stern Y. Structural MRI covariance patterns associated with normal aging and neuropsychological functioning. Neurobiol Aging 2007;28(2):284–295. [PubMed: 16469419]
28. Carbon M, Trost M, Ghilardi MF, Eidelberg D. Abnormal brain networks in primary torsion dystonia. Adv Neurol 2004;94:155–161. [PubMed: 14509669]
29. Petersen A, Zhao J, Carmichael O, Muller HG. Quantifying individual brain connectivity with functional principal component analysis for networks. Brain Connect 2016;6(7):540–547. [PubMed: 27267074]
30. Habeck C, Foster NL, Perneczky R, et al. Multivariate and univariate neuroimaging biomarkers of Alzheimer's disease. Neuroimage 2008;40 (4):1503–1515. [PubMed: 18343688]
31. Kaneko Y, Nozaki T, Yu H, et al. Normal T2 map profile of the entire femoral cartilage using an angle/layer-dependent approach. J Magn Reson Imaging 2015;42(6):1507–1516. [PubMed: 25917977]
32. Nieminen MT, Rieppo J, Silvennoinen J, et al. Spatial assessment of articular cartilage proteoglycans with Gd-DTPA-enhanced T1 imaging. Magn Reson Med 2002;48(4):640–648. [PubMed: 12353281]
33. Vincent KR, Conrad BP, Fregly BJ, Vincent HK. The pathophysiology of osteoarthritis: A mechanical perspective on the knee joint. PM R 2012; 4(5 Suppl):S3–S9. [PubMed: 22632700]

34. Everhart JS, Flanigan DC, Chaudhari AM, Siston RA. Tibiofemoral joint subchondral surface conformity: Individual variability with race and sexspecific trends. Knee 2016;23(5):770–776. [PubMed: 27288067]

35. Koh YG, Son J, Kwon OR, Kwon SK, Kang KT. Tibiofemoral conformity variation offers changed kinematics and wear performance of customized posterior-stabilized total knee arthroplasty. Knee Surg Sports Traumatol Arthrosc 2019;27(4):1213–1223. [PubMed: 29974167]

36. Haddock B, Fan AP, Uhlrich SD, et al. Assessment of acute bone loading in humans using [(18)F]NaF PET/MRI. Eur J Nucl Med Mol Imaging 2019;46(12):2452–2463. [PubMed: 31385012]

37. Haddock B, Fan AP, Jorgensen NR, Suetta C, Gold GE, Kogan F. Kinetic [18F]-fluoride of the knee in normal volunteers. Clin Nucl Med 2019;44(5):377–385. [PubMed: 30888996]

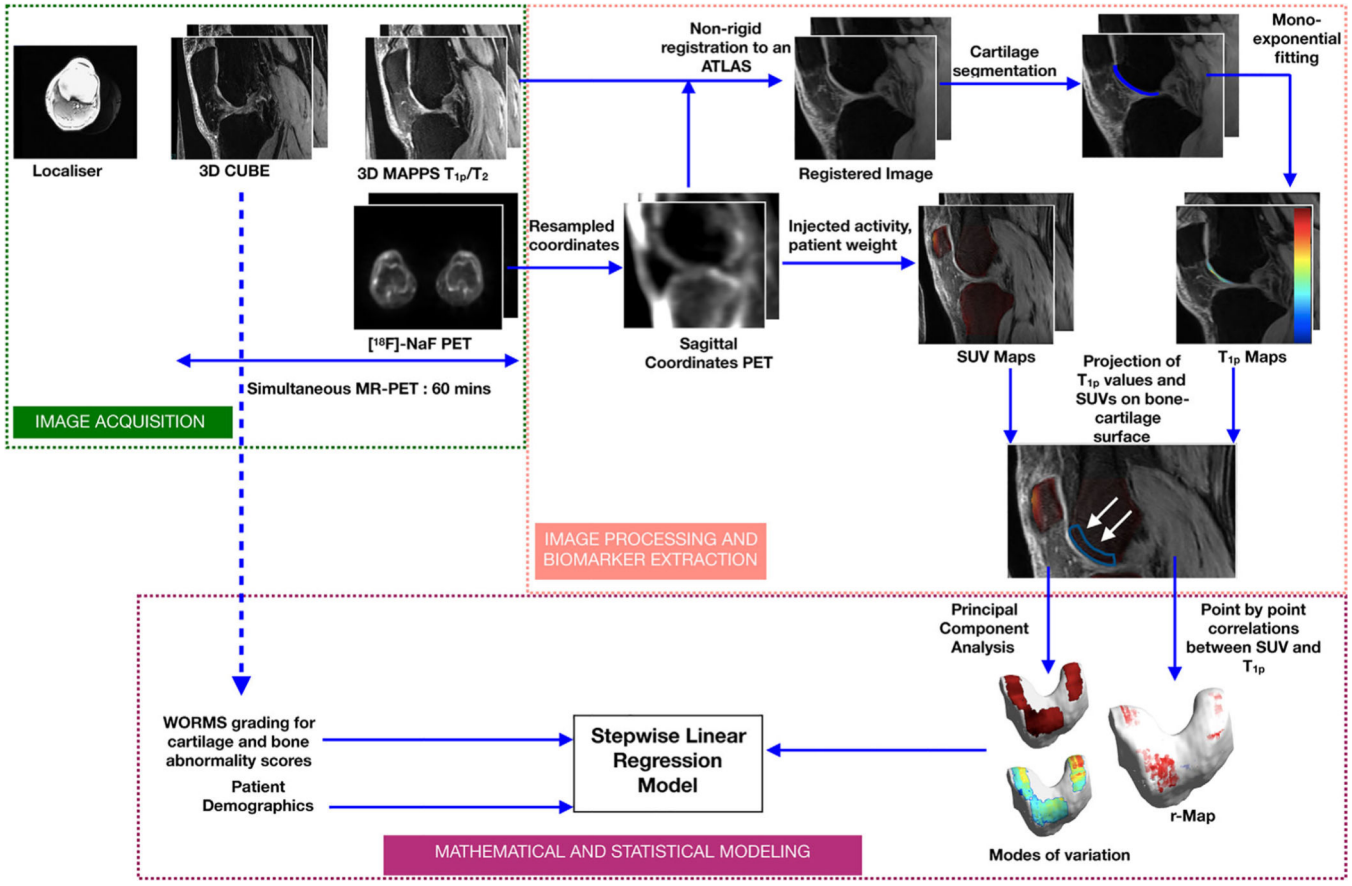

FIGURE 1:

Method pipeline. Image acquisition consisted of the 3D CUBE for morphological grading, 3D MAPPS sequence for cartilage segmentation, and $T_{1\rho}/T_2$ values. Along with the MRI, an [^{18}F]-NaF PET sequence was acquired to construct SUV maps in the same space as the $T_{1\rho}/T_2$ sequence. The $T_{1\rho}$ values and SUVs, recorded at cartilage and bone, respectively, were projected onto the bone–cartilage interface. These values were used to find point-by-point correlations, and more complex patterns of interactions between bone and cartilage were derived using PCA. A stepwise linear regression model was built to determine if these patterns can predict known manifestations of OA.

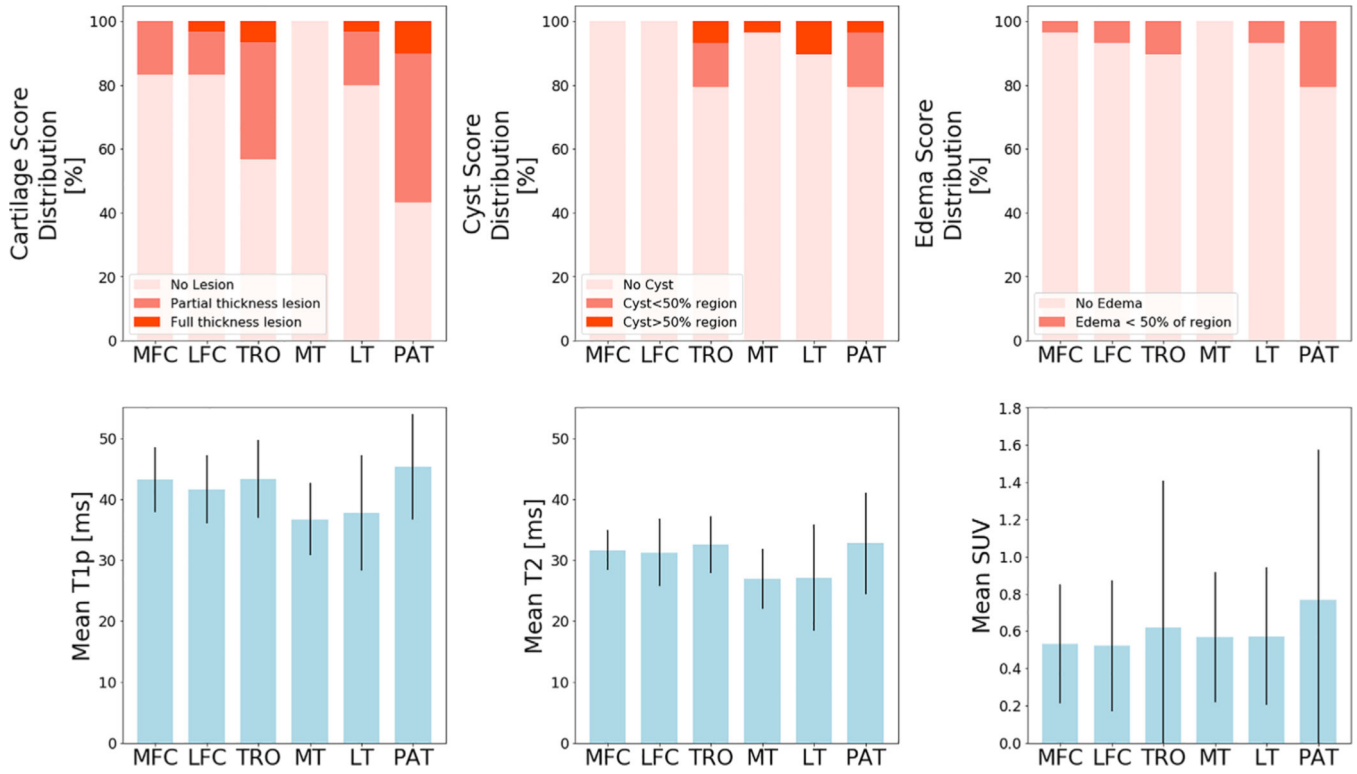

FIGURE 2:

(Top row) Distribution of the cartilage lesion scores, cyst scores, and bone marrow edema scores divided into three classes for cartilage and cyst and two classes for edema. (Bottom row) Mean $T_{1\rho}$ values (msec), mean T_2 values (msec), and mean SUVs in each knee compartment; medial femoral condyle (MFC), lateral femoral condyle (MFC), trochlea (TRO), medial tibial condyle (MT), lateral tibial condyle (LT), patella (PAT).

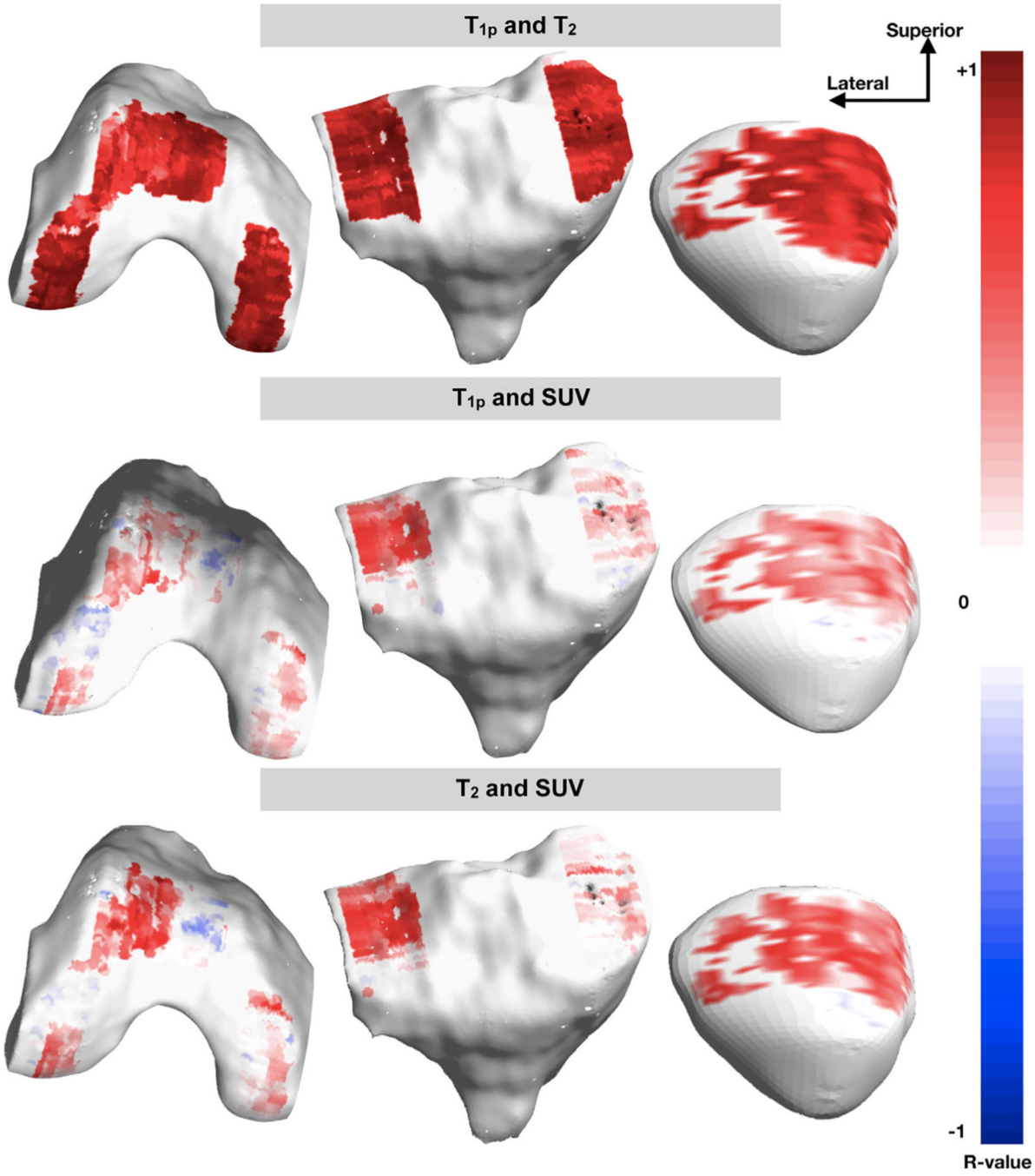

FIGURE 3:

Pearson correlation maP showing point-by-point correlation between the (top row) $T_{1\rho}$ and T_2 relaxation times, (middle row) $T_{1\rho}$ relaxation times and SUV, (bottom row) T_2 relaxation times and SUV, projected onto the same interface along the bone–cartilage surface in the (left–right) femur, tibia and patella. In all three bones, there is a strong positive correlation between $T_{1\rho}$ and T_2. There is weak-moderate positive correlation between $T_{1\rho}$ and SUV in the trochlea cartilage, the lateral tibia cartilage, and overall in the patella. There are small areas of weak-moderate negative correlations between $T_{1\rho}$ and SUV in part of the trochlea

cartilage and the outer edge of the lateral femoral cartilage. There is moderate-strong positive correlation between T_2 and SUV in the trochlea cartilage, the lateral tibia cartilage, and overall in the patella. There are small areas of weak-moderate negative correlations between T_2 and SUV in part of the trochlea cartilage.

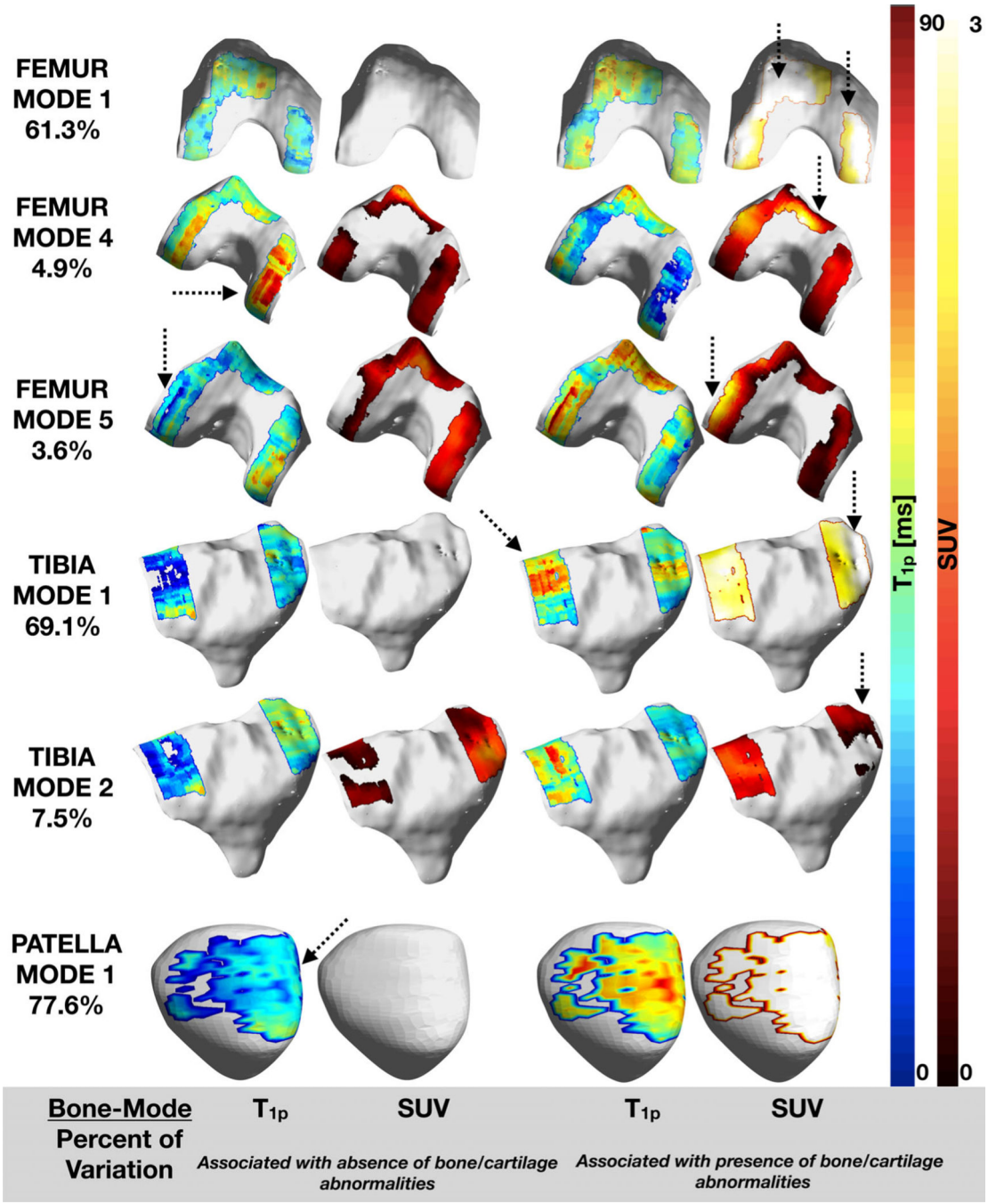

FIGURE 4:

Modes of variation in the femur, tibia and patella bones (modeled separately). ToP to bottom (modes) with percentage of variation of that mode listed under its label. Left and right columns: mode of variation ($T_{1\rho}$-SUV) visualized at −5 and +5 standard deviations.

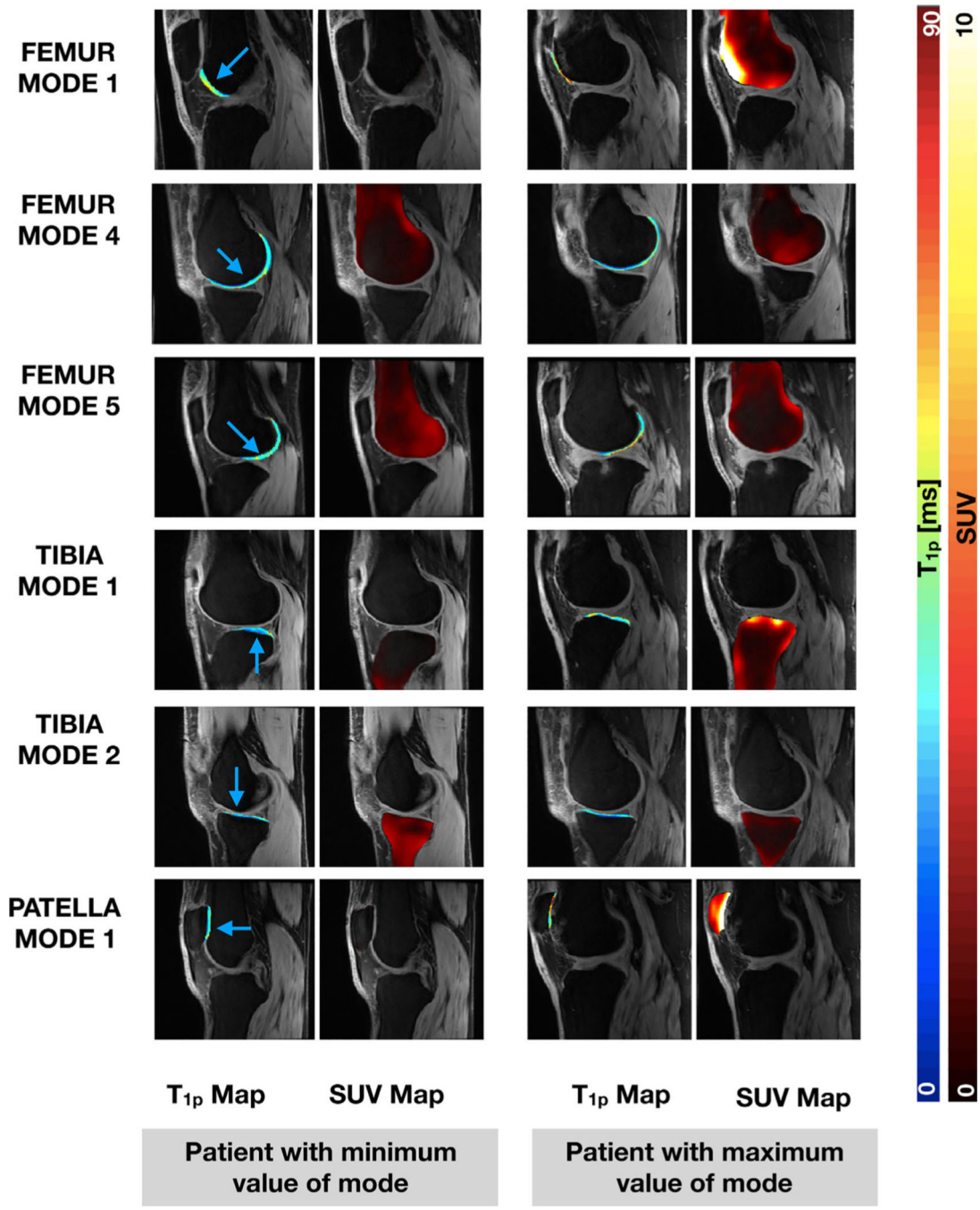

FIGURE 5:

$T_{1\rho}$ relaxation times and SUV maps overlaid on the first echo of the 3D $T_{1\rho}/T_2$ MAPSS sequence of patients with the minimum (left) and maximum (right) values of the modes that have associations with manifestations of OA in the femur, tibia, and patella. The blue arrow points to areas of the cartilage where the $T_{1\rho}$ and/or SUVs are different between the minimum and maximum value patient.

TABLE 1.

MRI Acquisition Parameters

MRI sequence	Acquisition prameters	Measurements
3 plane gradient echo		Localizer-for choosing coverage
3D CUBE FSE	TR/TE = 1500/26.69 msec, FOV =16 cm, Matrix Size = 384 × 384, Echo train = 32, slice thickness = 0.5 mm	WORMS grading
3D combined $T_{1\rho}/T_2$ MAPSS	TE = 0/12.87/25.69/51.39 msec, TSL = 0/10/40/80 msec, spin lock frequency = 500 Hz, FOV = 14 cm, Slice Thickness = 4 mm	Cartilage $T_{1\rho}/T_2$ relaxation time measurement, cartilage segmentation

FSE = fast spin-echo; FOV = field of view; WORMS = Whole-Organ Magnetic Resonance Imaging Score; TE = echo time; TR = repetition time; TSL = time of spin lock.

TABLE 2.

Percentage of Voxels That Displayed Significant ($P < 0.05$) Positive or Negative Correlations Between $T_{1\rho}$ Values and T_2 Values, $T_{1\rho}$ Values and SUVs, T_2 Values and SUVs in All Six Cartilage Compartments

		Femur			Tibia		Patella
	% of Voxels with significant correlation	**MFC**	**LFC**	**TRO**	**MT**	**LT**	**PAT**
Between $T_{1\rho}$ and T_2	Positive correlation	98	98	97	98	97	100
	Negative correlation	0	0	0	0	0	0
Between $T_{1\rho}$ and SUV	Positive correlation	4	13	11	5	45	40
	Negative correlation	0	1	1	0	0	0
Between T_2 and SUV	Positive correlation	8	16	35	6	53	60
	Negative correlation	0	0	1	0	0	0

SUV = standardized uptake value; $T_{1\rho} = T_{1\rho}$ relaxation times; $T_2 = T_2$ relaxation times; LFC = lateral femoral condyle; MFC = medial femoral condyle; TRO = trochlea; LT = lateral tibia; MT = medial tibia; PAT = patella.

TABLE 3.

Stepwise Linear Regression to Predict the Total Cartilage Lesion Score and the Total Bone Marrow Edema and Cyst Score Using the First Five Modes, Performed Separately in Each Bone (see Figs. S1 and S2 in the Supplementary Material for Full Version)

Cartilage lesion score			**Bone marrow edema + cyst**		
Femur			**Femur**		
	Estimate	***P* value**		**Estimate**	***P* value**
Intercept	−6.05	1.17E-01	Intercept	2.03	1.76E-06
MODE 1	0.14	3.78E-02	MODE 1	0.14	3.00E-04
MODE 5	1.71	3.99E-06	MODE 4	0.07	6.69E-01
AGE	0.19	7.70E-03	MODE 5	0.63	2.00E-04
MODE 1: MODE 5	−0.17	1.20E-03	MODE 1: MODE 4	0.03	3.87E-02
$R\text{-squared}_{adj}$ = 0.674, *P*-value = 2.16e-06			$R\text{-squared}_{adj}$ = 0.636, *P*-value = 7.84e-06		
Tibia			**Tibia**		
	Estimate	***P* value**		**Estimate**	***P* value**
Intercept	−8.29	1.01E-01	Intercept	2.03	2.50E-05
MODE 1	0.22	1.12E-02	MODE 1	0.18	1.40E-03
MODE 2	−0.73	7.60E-03	MODE 2	−0.54	1.50E-03
BMI	0.52	1.28E-02			
$R\text{-squared}_{adj}$ = 0.527, *P* value = 6.70e-05			$R\text{-squared}_{adj}$ = 0.453, *P* value = 1.48e-04		
Patella			**Patella**		
	Estimate	***P* value**		**Estimate**	***P* value**
Intercept	−11.07	4.92E-02	Intercept	−4.50	1.46E-01
MODE 1	0.24	2.44E-02	MODE 1	0.22	7.00E-04

Cartilage lesion score			Bone marrow edema + cyst		
Femur			Femur		
	Estimate	*P* value		Estimate	*P* value
BMI	0.63	6.50E-03	BMI	0.26	3.74E-02
R-squared$_{adj}$ = 0.404, *P*-value = 4.58e-04			R-squared$_{adj}$ = 0.479, *P*-value = 8.01e-05		

TABLE 4.

Stepwise Linear Regression to Predict the Total Cartilage Lesion Score and the Total Bone Marrow Edema and Cyst Score Using the Mean $T_{1\rho}$ Values and SUVs, Performed Separately in Each Bone (see Figs. S1 and S2 in the Supplementary Material for Full Version)

Cartilage lesion score			**Bone marrow edema + cyst**		
Femur			**Femur**		
	Estimate	***P* value**		**Estimate**	***P* value**
Intercept	−16.55	6.00E-04	Intercept	−8.79	7.80E-03
SUV - TRO	3.35	1.00E-04	SUV - TRO	1.74	2.90E-03
$T_{1\rho}$ - LFC	0.46	1.00E-04	$T_{1\rho}$ - LFC	0.24	3.20E-03
$R\text{-squared}_{adj}$ = 0.598, *P*-value = 2.72e-06			$R\text{-squared}_{adj}$ = 0.421, *P*-value = 3.11e-04		
Tibia			**Tibia**		
	Estimate	***P* value**		**Estimate**	***P* value**
Intercept	32.44	1.02E-01	Intercept	−10.97	2.09E-03
$T_{1\rho}$ - LT	−1.18	3.36E-02	$T_1\rho$ - LT	0.16	5.10E-03
BMI	−1.36	6.47E-02	BMI	0.28	3.60E-02
$T_{1\rho}$ - LT: BMI	0.05	9.20E-03			
$R\text{-squared}_{adj}$ = 0.623, *P*-value = 4.19e-06			$R\text{-squared}_{adj}$ = 0.398, *P*-value = 5.26e-04		
Patella			**Patella**		
	Estimate	***P* value**		**Estimate**	***P* value**
Intercept	−12.54	2.23E-02	Intercept	−6.02	5.50E-02
SUV - PAT	2.25	1.95E-02	SUV - PAT	1.86	1.50E-03
BMI	0.61	7.10E-03	BMI	0.26	4.11E-02

Cartilage lesion score			Bone marrow edema + cyst	
Femur			Femur	
	Estimate	*P* value	Estimate	*P* value
$R\text{-squared}_{adj}$ = 0.413, *P*-value = 3.76e-04			$R\text{-squared}_{adj}$ = 0.449, *P*-value = 1.66e-04	

SUV = standardized uptake value; T_1P = T_1 *P* relaxation times; TRO = trochlea; LFC = lateral femoral condyle; LT = lateral tibia; PAT = patella.